Journal of Marine Science and Application (2025) 24: 21-34
https://doi.org/10.1007/s11804-024-00481-8

REVIEW

A Review of the Hydrodynamic Damping Characteristics of Blade-like Structures: Focus on the Quantitative Identification Methods and Key Influencing Parameters

Yongshun Zeng[1], Zhaohui Qian[1], Jiayun Zhang[2] and Zhifeng Yao[2,3]

Received: 28 January 2024 / Accepted: 04 April 2024

Abstract

Ocean energy has progressively gained considerable interest due to its sufficient potential to meet the world's energy demand, and the blade is the core component in electricity generation from the ocean current. However, the widened hydraulic excitation frequency may satisfy the blade resonance due to the time variation in the velocity and angle of attack of the ocean current, even resulting in blade fatigue and destructively interfering with grid stability. A key parameter that determines the resonance amplitude of the blade is the hydrodynamic damping ratio (HDR). However, HDR is difficult to obtain due to the complex fluid–structure interaction (FSI). Therefore, a literature review was conducted on the hydrodynamic damping characteristics of blade-like structures. The experimental and simulation methods used to identify and obtain the HDR quantitatively were described, placing emphasis on the experimental processes and simulation setups. Moreover, the accuracy and efficiency of different simulation methods were compared, and the modal work approach was recommended. The effects of key typical parameters, including flow velocity, angle of attack, gap, rotational speed, and cavitation, on the HDR were then summarized, and the suggestions on operating conditions were presented from the perspective of increasing the HDR. Subsequently, considering multiple flow parameters, several theoretical derivations and semi-empirical prediction formulas for HDR were introduced, and the accuracy and application were discussed. Based on the shortcomings of the existing research, the direction of future research was finally determined. The current work offers a clear understanding of the HDR of blade-like structures, which could improve the evaluation accuracy of flow-induced vibration in the design stage.

Keywords Blade fatigue; Hydrodynamic damping ratio; Identification method; Affecting factors; Prediction formula

1 Introduction

The abundance of ocean energy can satisfy nearly five times the world's energy demand (Chen et al., 2018). Especially for tidal and current marine energy, the economically exploitable resource was estimated at 1 000 and 180 TWh per year, respectively (Chen et al., 2018; Xie et al., 2020) As shown in Figure 1, energy converters, such as the tidal current turbine (Nachtane et al., 2020) and marine current turbine (Xie et al., 2020), were widely used to generate electricity. The core component is the blade, which transfers the kinetic energy of the flow to the mechanical energy of the runner (Zhu et al., 2022). The reliability analysis of the blade is crucial due to the expensive costs and difficulty of maintenance for the energy converter in the ocean.

Article Highlights

- The processes of experimental and simulation methods are comprehensively described to identify the HDR.
- The key typical flow parameters that affect the HDR of blade-like structures are summarized.
- The theoretical derivation and semi-empirical prediction formulas of HDR are introduced.

✉ Zhifeng Yao
yzf@cau.edu.cn

[1] Department of Energy and Power Engineering, Tsinghua University, Beijing 100084, China

[2] College of Water Resources and Civil Engineering, China Agricultural University, Beijing 100083, China

[3] Beijing Engineering Research Center of Safety and Energy Saving Technology for Water Supply Network System, Beijing 100083, China

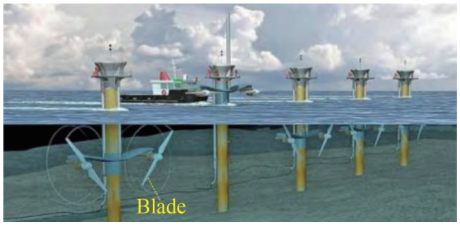

Figure 1 Concept of marine current turbine farm (Chen et al., 2018)

The safety and stable operation of the energy converter are seriously threatened by the blade fault, such as the blade crack in Figure 2 (Xie et al., 2020). Xie et al. (2020) indicated the relationship between the root cause and the flow environment, such as the rapid change in the surround-

ing flow velocity (Nicholls-Lee et al., 2011; Chen et al., 2012). In addition, the attack of angle (AOA) was variable due to changes in the ocean current direction (Wang et al., 2021b; Bai et al., 2022). This variation leads to changes in blade force (Wang and Wan, 2020). In particular, the power density substantially increased with the rising velocity, as shown in Table 1. Moreover, changes in the trailing edge shedding frequency can be attributed to variations in flow velocities and AOAs (Wu et al., 2022). In this situation, satisfying the blade resonance is possible. Thus, the amplitude of vortex-induced vibration can be increased by more than 100 times, resulting in serious blade damage (Zobeiri et al., 2012; Zeng et al., 2021b).

Figure 2 Picture of a blade crack in the actual engineering (Xie et al., 2020)

Table 1 Power density at different conditions for a marine current (Chen et al., 2018; Fraenkel, 2002)

Velocity (m/s)	1	1.5	2	2.5	3
Power density (kW/m^2)	0.52	1.74	4.12	8.05	13.9

As shown in Figure 3, the hydrodynamic damping ratio (HDR) is a key factor in controlling the resonance amplitude of underwater blades (Coutu et al., 2012). Accurately calculating the deflection and stress of a blade under external excitations is crucial in the design stage. With the widespread exploitation of ocean energy and increasing concerns regarding failure assessment in the early life of blades, Trivedi (2017) and Dehkharqani et al. (2018) carefully performed literature reviews to introduce the fluid–structure interaction (FSI) behaviors of blades. Available excitation methods for the underwater blades and the corresponding responses were summarized, and the effect of free-stream velocity on the HDR was extensively analyzed (Trivedi, 2017; Dehkharqani et al., 2018). However, detailed descriptions of the specific processes of HDR acquisition methods were lacking, and systematic comparisons between various methods were also insufficient. In addition, with the development of HDR acquisition methods, a considerable amount of HDR data has been recently reported with various flow parameters (such as cavitation and rotation conditions), and a comprehensive understanding of HDR must be realized (Chen et al., 2020b; Zhou et al., 2023). Moreover, the HDR is an FSI parameter that requires tedious preliminary work and a long time to determine the HDR of a blade-like structure (Kohtanen and Davis, 2019; He et al., 2014). Therefore, from the viewpoint of actual engineering, establishing a prediction formula to determine the HDR in the design stage is preferred.

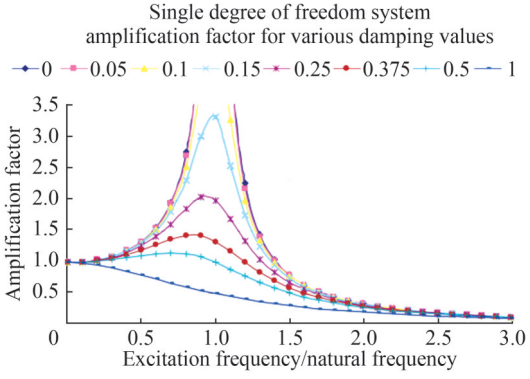

Figure 3 Role of the damping ratio in controlling the resonance amplitude (Coutu et al., 2012)

This study aims to assess the hydrodynamic damping characteristics of blade-like structures, focusing on the following three aspects: 1) introducing the experimental and simulation methods to quantitatively obtain the HDR; 2) summarizing the typical flow parameters that affect the HDR; 3) proposing the existing empirical prediction formulas for HDR.

2 Definition of HDR

Damping is the removal of energy from a vibratory system (Crandall, 1970), and the damping ratio is a parameter that reflects the capability to dissipate energy during oscillations (Kaminer and Kavitskii, 1976). Considering the damping ratio, the motion equation of a single-degree-of-freedom linear system is as follows (Yao et al., 2014; Gauthier et al., 2017):

$$m\ddot{y} + c\dot{y} + ky = F(t) \tag{1}$$

where m, c, and k are the mass, damping, and stiffness coefficients, respectively; y is the displacement; the superscripts with one point and two points represent the first- and second-order derivatives of time, respectively; and $F(t)$ is the external load.

The vibration does not move periodically and returns to the equilibrium position at the fastest speed when the damping coefficient reaches a critical value. This damping coefficient is called the critical damping coefficient, as shown below (Bulatovic, 2002):

$$c_r = 2\sqrt{km} \tag{2}$$

The total damping ratio is defined as the ratio between the damping and critical damping coefficients (Gauthier et al., 2017):

$$\zeta_t = c/c_r \tag{3}$$

The total damping ratio can be divided into three categories (Trivedi, 2017; Dehkharqani et al., 2018): 1) the HDR, or fluid-added damping ratio; 2) the structural, friction, or Coulomb damping ratio; 3) the material, or hysteretic damping ratio. In flowing water, the HDR was substantially larger than the structural and material damping ratios (Trivedi, 2017). Therefore, the total damping ratio of structures in water was regarded as the HDR in some references (Roth et al., 2009; Bergan et al., 2018b). In some previously published works (Reese, 2010; Blake and Maga, 1973), the HDR was also defined as the only contribution of the flowing water; that is, the HDR = 0 in still water. The HDR in the current study is interpreted as the dissipated energy capability of the water (Trivedi, 2017; Dehkharqani et al., 2018) as follows:

$$\zeta_h = \zeta_t - \zeta_s \tag{4}$$

where ζ_h is the HDR and ζ_s is the damping ratio in the structure (includes the structural and material damping).

3 Quantitative identification methods of HDR

3.1 Experiment methods

As shown in Figure 4, the experimental measurement of HDR comprises the following three parts: structural excitation, vibration response acquisition, and HDR calculation. The structural excitation type can be divided into impulse and sweep excitations. The vibration response acquisition can also be divided into contact and noncontact measurements.

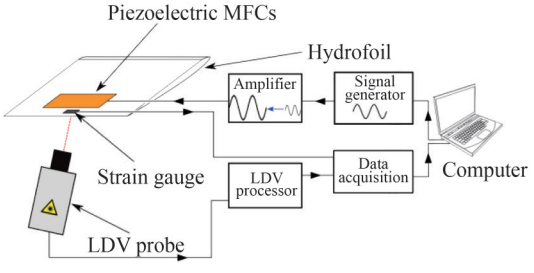

Figure 4 Schematic of the vibration measurement of a hydrofoil (Bergan et al., 2018b)

3.1.1 Structural excitation

A transient load is applied to the structure through impulse excitation, thereby simultaneously stimulating multiple modes of the structure. The HDR is theoretically measured based on the gradually decayed vibration amplitude after excitation removal. As early as the 1970s, Blake et al. (1972; 1973) used the hammer as a traditional impulse excitation tool for hydrofoil excitation. In recent years, semi-submerged plates and hydrofoils still use the hammer due to its reliability and convenience (Xiu et al., 2018). Structure excitation without disturbing the flow is difficult for a hammer in fully submerged water. In this situation, Roth et al. (2009) and Roth (2012) applied impulse excitation using the spark-generated bubble. Specifically, bubble collapse generated strong shock waves, which then traveled toward the blade and provided impulse excitation (Roth et al., 2009).

The excitation frequency continuously changes for the sweep method and triggers the resonance, and the HDR can be measured in accordance with the resonance amplitude of the structure. The piezoelectric macrofiber composite actuator (MFC) (Bergan et al., 2018b; Seeley et al., 2012) and the piezoelectric ceramic material patches (PZT) are the most commonly used devices (Presas et al., 2014). The signal generator was frequently used together to produce sweep voltage, which was then fed to MFC or PZT through a power amplifier (Zeng et al., 2022a). The operating voltage of MFC and PZT ranges from −500 V to 1 500 V (Seeley et al., 2012) and from −200 V to 400 V (Yao et al., 2014), respectively, indicating the MFC has the potential to produce remarkable structural deformations. For example, Bergan et al. (2018b) adapted the MFC to excite the hydrofoil with two fixed sides. The PZT has the advantage of its small size and flexible arrangement, enabling its embedment in the structure and thus avoiding interference with the flow(Torre et al., 2013; 2014; Cha et al., 2016). Especially in rotating conditions, Presas et al. (2015; 2016) and Zeng et al. (2023a) realized the controllable excitation of a rotating disk by combining PZT and slip rings. Electromagnetic technology has also been recently used to excite underwater structures. For example, Weder et al. (2019) placed a permanent magnetic cube (mass 1.05 g) on a disk and then applied excitation using the electromagnetic coil, with an excitation frequency ranging from 0 to approximately 2 388 Hz.

3.1.2 Vibration response acquisition

The most commonly used contact vibration measurement devices are acceleration sensors, which are typically attached to or embedded in the surface of a structure. The reliability of these sensors was generally recognized and was widely used, such as in experiments with hydrofoils (Blake and Maga, 1973), disks (Presas et al., 2017), and blades (Chen et al., 2020a). PZT has a voltage output after deflection; thus, this device was also used for vibration response acquisition. For example, Yao et al. (2014) measured the vibration of the hydrofoil at a velocity ranging from 3 m/s to 21 m/s using the PZT. Similarly, Presas et al. (2019) adapted the PZT as a sensor to obtain the vibration response of the runner (with a radius of 200 mm). Torre

et al. (2013) and Zeng et al. (2021b) compared the vibration response results of the hydrofoil obtained by the acceleration sensor and PZT, respectively, and found that the natural frequencies are in good agreement.

A noncontact vibration measurement device does not interfere with the flow on the one hand and does not affect the structural properties on the other. The laser Doppler vibrometer (LDV) is a typical noncontact vibration measurement device, and the basic measurement principle is shown in Figure 5 (Zobeiri, 2012). Xiu et al. (2018), Roth et al. (2009), Kohtanen et al. (2019), Seeley et al. (2012), and Bergan et al. (2018a) obtained the time evaluation of the vibration response of nonrotating structures, such as plates and hydrofoils. In the rotating condition, Weder et al. (2019) designed an interesting system and then measured the vibration response of the rotating disk using LDV, as shown in Figure 6. In this figure, a polar scan unit was developed and co-rotated with the rotor assembly, and the light produced by the LDV was then reflected by the mirror of the scanner. In addition to the LDV, fiber optic technology was also used for displacement measurement of the hydrofoils, specifically for simultaneous measurement of multiple marking points (Pernod et al., 2019; Maung et al., 2021). This finding indicates the good applicability of fiber optic technology in characterizing the mode shape of the structure.

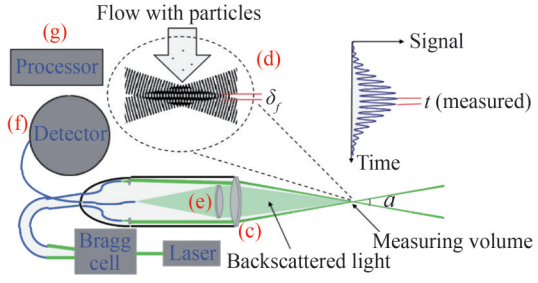

Figure 5 Basic measurement principle of LDV (Zobeiri, 2012). (a) Laser source; (b) Brag cell; (d) Measurement volume; (e) Receiving lens; (f) Photodetector; (g) Signal processing

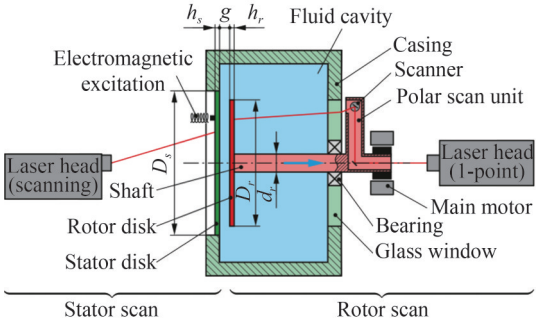

Figure 6 Schematic of the vibration measurement of a rotating disk using the LDV (Weder et al., 2019)

3.1.3 HDR identification

The identification method of HDR is closely related to the structural excitation method. The free vibration of a single-order mode is finally obtained for the impulse excitation. In this situation, the logarithmic decay method (Younes et al., 2007) and the Hilbert transform method (Jacobson et al., 2019) are often applied to identify the HDR of the underwater vibrating hydrofoil. The forced vibration is finally obtained for the sweep method, and the HDR is identified based on the vibration amplitude near the resonance frequency. Therefore, Seeley et al. (2012) and Zeng et al. (2022b) fitted the resonance curve using the dynamic amplification method and then obtained the HDRs. In addition, the half-power bandwidth method and the circle fitting method (Silva, 2000) were employed to identify the HDRs of the forced vibrations.

1) For the logarithmic decay method, the total damping can be identified by fitting the discrete points of the free vibration as follows:

$$y(t) = A\mathrm{e}^{-\zeta_t\omega_n}\sin\left(\omega_d t + \varphi\right) \tag{5}$$

where $y(t)$ is the instant displacement, A is the amplitude, t refers to the time, ω_d is the damped angular natural frequency, and φ is the initial phase.

2) Considering the Hilbert transform method, the harmonic conjugate of the original signal $y(t)$ is obtained as follows (Jacobson et al., 2019):

$$\tilde{y}(t) = \frac{1}{\pi}\int_{-\infty}^{\infty}\frac{y(\tau)}{t-\tau}\mathrm{d}\tau \tag{6}$$

where τ is the time scale.

The vibration response can then be expressed as a function of a harmonic conjugate pair, as shown below:

$$Y(t) = y(t) + \tilde{y}(t) = A(t)\mathrm{e}^{(i\theta(t)t)} \tag{7}$$

where $A(t) = \mathrm{e}^{\left(-\zeta_t(t)\omega_n(t)t\right)}$ is the instantaneous envelope and $\theta(t)$ is the instantaneous vibration phase.

The instantaneous natural frequency can be calculated as follows:

$$\omega_n(t) = \mathrm{d}\theta(t)/\mathrm{d}t \tag{8}$$

The instantaneous damping ratio can finally be calculated:

$$\zeta_t(t) = -\frac{1}{\omega_n(t)}\frac{\mathrm{d}\ln A(t)}{\mathrm{d}t} \tag{9}$$

3) The dynamic amplification method fits the frequency–amplitude curve to obtain the HDR as shown below (Yao et al., 2014):

$$\beta = \frac{1}{\sqrt{\left(1-\omega_e^2/\omega_n^2\right)^2 + 4\zeta_t^2\omega_n^2/\omega_e^2}} \tag{10}$$

where β is the dynamic amplification factor and ω_e is the excitation angular frequency.

4) The β reaches its maximum value, that is, $\beta_0 = 1/(2\zeta_t)$, when the ω_e coincides with the ω_n. The half-power bandwidth is defined as the width of the frequency–amplitude curve if the amplitude is $1/(\sqrt{2}\,\beta_0)$. A function can then be established as follows (Silva, 2000):

$$\frac{1}{\sqrt{\left(1-\omega_e^2/\omega_n^2\right)^2+4\zeta_i^2\omega_n^2/\omega_e^2}}=\frac{1}{2\sqrt{2}\,\zeta_t} \tag{11}$$

Assuming the $0<\zeta_t<1/2\sqrt{2}$ and $\zeta^4\to 0$, Equation (11) can be written as:

$$\zeta_t=\frac{\Delta\omega}{2\omega_n}=\frac{\left|\omega_1-\omega_2\right|}{2\omega_n} \tag{12}$$

where the $\Delta\omega$ is the half-power bandwidth; ω_1 and ω_2 are the frequencies, where $\beta = 1/(\sqrt{2}\,\beta_0)$.

5) The circle fit method must construct the frequency response function as follows:

$$H\left(\omega_e\right)=\frac{y\left(\omega_e\right)}{F\left(\omega_e\right)}=H_r\left(\omega_e\right)+\mathrm{j}H_i\left(\omega_e\right) \tag{13}$$

where $y\left(\omega_e\right)$ and $F\left(\omega_e\right)$ are the FFT of vibration response and excitation signal, respectively. $H_r\left(\omega_e\right)$ and $H_i\left(\omega_e\right)$ are the real and imaginary parts of the frequency response function, respectively.

The resonant peak of a single modal will appear as a circle based on the plotted $H_r\left(\omega_e\right)$ and $H_i\left(\omega_e\right)$ in a complex plane (i.e., Nyquist plot). The total damping ratio can then be identified as follows (Bergan et al., 2018a; Anthony et al., 2012):

$$\zeta_t=\frac{\omega_a^2-\omega_b^2}{2\omega_n}\frac{1}{\omega_a\tan\left(0.5\Delta\theta_a\right)+\omega_b\tan\left(0.5\Delta\theta_b\right)} \tag{14}$$

where $\Delta\theta$ represents the phase difference from the resonance point, and the subscripts *a* and *b* represent the points close to the resonance point.

3.1.4 Evaluation of experimental methods

Considering the excitation method, the application of a hammer to a transient force is recommended for the semi-submerged structure due to its convenience and non-interference with the flow. If the blade rotates in water, then the embedded MFC and PZT are proven reliable. Especially in prototype blade testing, MFC should be used with a power amplifier to produce sufficient structural deformations.

Considering the vibration response acquisition, the LDV is initially recommended because of its non-interference with the FSI behaviors and easy calibration between voltage and displacement signals. The LDV can even be adopted under rotating conditions in combination with a polar scan unit. However, the LDV also has its drawbacks, such as its unsuitability for an opaque environment. In this situation, the embedded PZT in the blade is recommended as a sensor due to its capability to follow the structural movement. Notably, the PZT is sensitive to temperature and relatively fragile (Dehkharqani et al., 2018) Thus, the application of PZT must be within the allowable voltage range.

Considering HDR identification, Zrayka and Mucchi (2019) conducted a comparison among several methods in a MATLAB environment, and the cycle fit method was recommended due to its good robustness. Jacobson et al. (2019) used self-compiled functions to control the damping ratio of vibration signals and discussed the applicability of various HDR identification methods, such as multicomponent signals, short signal intervals, and high-noise input signals, under adverse conditions. Zeng et al. (2022b) measured the vibration response of a hydrofoil and systematically compared five identification methods of HDR, as shown in Table 2. In the table, M1–M5 refer to the logarithmic decay, Hilbert transform, dynamic amplification, half-power bandwidth, and circle fitting methods. The results showed similarities in the accuracy and uncertainty of the different methods. However, considering the logarithmic decay and half-power bandwidth methods are simple to use and fast to implement according to Equations (5) and (12), these methods should be used in free and forced vibration, respectively. The Hilbert transform method is recommended for the situation with time-varying HDR.

Table 2 Comparison of different damping ratio identification methods (Zeng et al., 2022b)

Method	M1	M2	M3	M4	M5
Ave HDR	0.015	0.014 9	0.016 4	0.015 5	0.016
Uncertainty	3.81%	6.95%	6.72%	7.65%	2.21%

3.2 Simulation methods

The numerical simulation methods of HDR have also received extensive attention to obtain vibration signals conveniently and analyze the internal flow mechanism. These methods mainly include the unsteady vortex lattice method (UVLM), the modal work approach, and the two-way FSI method.

3.2.1 Unsteady vortex lattice method

The UVLM is based on potential flow theory and assumes structural vibration in an inviscid, incompressible, and irrotational fluid (Kohtanen and Davis, 2019) The HDR can then be calculated by performing the following two steps:

1) The unsteady force distribution on the structure can be calculated based on the circulation of vortex singularities over the structure and the wake (Kohtanen and Davis, 2019;

Chen et al., 2020a) as follows:

$$\boldsymbol{F} = \sum_{a=1}^{M}\sum_{b=1}^{N} -\left(\Delta p \Delta S\right)_{ab} \boldsymbol{n}_{ab} \tag{15}$$

where $\boldsymbol{F}$ is the unsteady force vector; M and N represent the node number of chordwise and spanwise, respectively; subscripts a and b determine the node position; Δp is the pressure difference; ΔS is the area; and $\boldsymbol{n}$ is the normal vector.

2) The HDR can be determined by combining the vibration information and the unsteady force as follows (Chen et al., 2020a):

$$\zeta_{h,i} = \frac{\boldsymbol{F}_{\text{damping}}}{2m_i\omega_{n,i}v} \tag{16}$$

$$\boldsymbol{F}_{\text{damping}} = \boldsymbol{F}\sin\phi \tag{17}$$

where $\boldsymbol{F}_{\text{damping}}$ is the damping force induced by the phase difference (ϕ) between the unsteady force and motion, m is the modal mass of the ith modal, ω_n is the angular natural frequency, subscript i represents the ith modal, and v is the vibrating velocity.

3.2.2 Modal work approach

The ratio of the dissipated energy in a vibrating cycle to the total energy of the vibrating system is calculated using the modal work approach (Monette et al., 2014; Nennemann et al., 2016). This approach only transferred the information of the structural field to the flow field; thus, this approach is also called the one-way-coupled simulation method (Tengs, 2019; Wang et al., 2021a).

Three steps should be conducted to calculate the HDR. 1) The modal analysis (Liang et al., 2007) of the structure is performed to calculate the mode shape and corresponding natural frequency. 2) The unsteady CFD simulation of the flow domain aims to determine the unsteady pressure and stress on the structure. In particular, the mode motion of the structure was set as the boundary condition in this step using the dynamic mesh technology, as shown in Figure 7 (Wang et al., 2021a). 3) The HDR can be obtained as follows (Gauthier, 2017; Čupr et al., 2019):

$$\zeta_{h,i} = \frac{\Delta W}{2\pi\left(m_{s,i} + m_{f,i}\right)\omega_{nf,i}^2 A_0^2} \tag{18}$$

$$\Delta W = \frac{1}{N}\int_0^{2\pi N/\omega_{nf}} \iint_s \left(p\boldsymbol{n} + \boldsymbol{\tau}\right)\mathrm{d}s\,\dot{y}\mathrm{d}t \tag{19}$$

where ΔW is the dissipated energy in a vibrating cycle; m_s and m_f are the modal mass in air and water, respectively; ω_{nf} is the angular natural frequency in water; A_0 is the amplitude of the mode shape; and $\boldsymbol{\tau}$ is the shear stress vector. ΔW is the area integral of the "Wall Power Density" over the moving wall using the ANSYS CFX code.

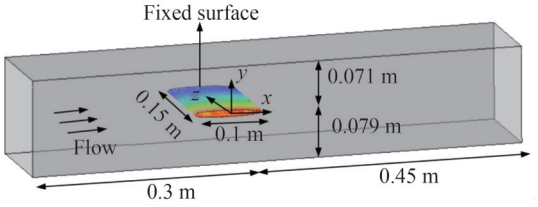

Figure 7 Mode motion is set as the boundary condition for the modal work approach (Wang et al., 2021a)

3.2.3 Two-way FSI method

The unsteady CFD and unsteady computational structural dynamics are combined in the two-way FSI method. In particular, the structural vibration information was transmitted to the flow field through the FSI surface, and the flow pressure was transmitted back to the structure field (Liaghat et al., 2014; Zeng et al., 2019a).

Specifically, this method can also be divided into three steps. 1) An impulse excitation was applied to the surface of the structure to induce the structural vibration, as shown in Figure 8(a) (Zeng et al., 2019b). 2) As shown in Figure 8(b), the vibration response acquisition was generally based on dynamic mesh technology, and the vibration response on the FSI interface was monitored. 3) The HDR calculation uses the logarithmic decay formula (20) to fit the peak points of the vibration response (Zeng et al., 2019a; Liu et al., 2015).

$$y(t) = A\mathrm{e}^{-\zeta_i\omega_n t} \tag{20}$$

where $y(t)$ is the instant displacement, A is the amplitude, and t refers to the time.

3.2.4 Accuracy and applicability

The UVLM theoretically performs various simplifications on the flow and potentially efficiently obtains the HDR at the design stage. However, only simple structures such as plates and 2D blades currently benefit from this method, and its accuracy is limited in some high-velocity situations. For example, Kohtanen and Davis (2019) used the UVLM to obtain the HDRs of a plate for the first four modes. In quiescent water, compared with the experimental results, the relative error was within 11.2%. Meanwhile, the relative error remained below 30% for most modes of flowing water. Similarly, Chen et al. (2020a) obtained the HDRs of a blade at different rotating speeds using the UVLM. The simulation results are consistent with experimental data at some low rotating speed conditions, while the HDR was overestimated by UVLM at some high rotating speed conditions.

Regarding the modal work approach, the fluid pressure and shear stress can be accurately captured despite the simplified vibration mode of the structure. In the case of a hydrofoil, Nennemann et al. (2016) obtained the HDRs for the first-order bending and torsional modes and generally achieved good comparisons between simulation and exper-

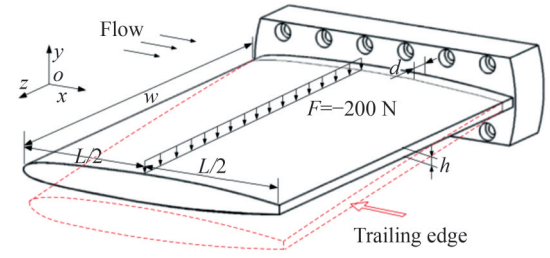

(a) Excitation method (Zeng et al., 2019b)

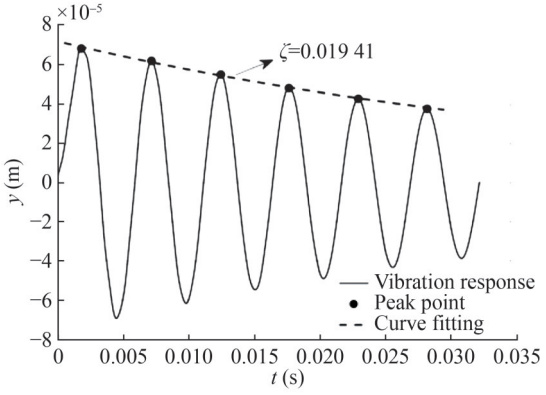

(b) Time evolution of vibration signal and identification of damping ratio (Zeng et al., 2019a)

Figure 8 Calculation of HDR using the two-way FSI method

imental results with relative error within 20%. Gauthier et al. (2017) also found that the error of the HDRs for the first bending mode was within 10%, as shown in Figure 9. Therefore, the modal work approach was widely used for the blade-like structures. Tengs et al. (2019) obtained the HDRs of hydrofoils when the velocity ranged from 2.5 m/s to 45 m/s, which was substantially higher than the experimental flow velocity. Moreover, Gauthier et al. (2017) and Zhang et al. (2021) used the modal work approach to predict the HDRs of a Kaplan turbine runner at different flow rates, indicating the application potential of this method to rotating hydraulic machinery with complex structures. Notably, the modal work approach was sensitive to the amplitude of the vibrating structure. For example, the error of predicted HDR can reach 300% when the deflection of the hydrofoil is increased from 0.05 mm to 2.5 mm, and a two-way FSI is necessary in this situation (Tengs, 2019).

Compared with other methods, the two-way FSI method is theoretically more complete, thereby providing higher accuracy. However, the solution of the structural vibration equations produced a numerical damping ratio (Liaghat, 2014; Aquelet et al., 2003). The default value of the numerical damping ratio is 0.1 in the ANSYS code, which is unsuitable for all calculation settings. For example, Liaghat et al. (2014) indicated that a small numerical damping ratio necessitated a large time step, easily resulting in the calculation divergence. Zeng et al. (2019a) conducted an independent analysis of the time step and numerical damping ratio and obtained the HDRs of a hydrofoil. They found that the relative error was within 8.84% when the velocity ranged from 2 m/s to 20 m/s. In addition to calculation accuracy, this study also focused on calculation time. A total of 94 hours were required at one flow condition with 16 cores for the simulation of the HDR of a hydrofoil (Zeng et al., 2019a), which was approximately 15 times that of the modal work approach (Zeng et al., 2020).

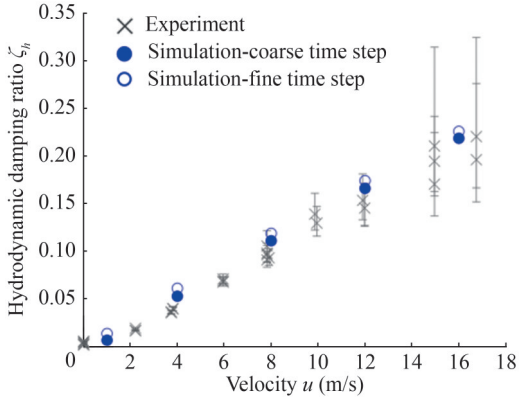

Figure 9 HDRs of a hydrofoil obtained by the experiment and the modal work approach, and the relative error is within 10% (Gauthier et al., 2017)

Therefore, considering the calculation accuracy and efficiency, the modal work method is recommended for complex structures. Meanwhile, the two-way FSI method is recommended for cases of large deformation or with strict requirements on calculation accuracy.

4 Influencing parameters of HDR

4.1 Effect of incoming flow velocity

Theoretically, flow environments have a considerable impact on the energy dissipation capability of the vibration system (Vandiver and Chung, 1989; Chaplin and Subbiah, 1998). Previously published literature revealed three relationships between flow velocity and the HDR.

1) The HDR damping ratio increased linearly with rising velocity. In the case of a hydrofoil, based on experiments performed in 1976, Kamier and Kavitskii (1976) obtained the linear relationship between the HDR of the bending mode and flow velocity. Similarly, Seeley et al. (2012) reproduced these experiment results for three different hydrofoils (as shown in Figure 10) and obtained the slopes between HDR and velocity. In addition to the hydrofoil, a cylinder also demonstrated the same behavior as the HDR (Yang et al., 1985; Chaplin, 2000).

2) The HDR damping ratio remained constant as the velocity increased. Especially for some low-velocity conditions, the results of some experiments performed on the hydrofoil (Rankl et al., 2004; Roth et al., 2009; Yao et al., 2014), tube (Chen and Jendrzejczyk, 1981), plate (Santo,

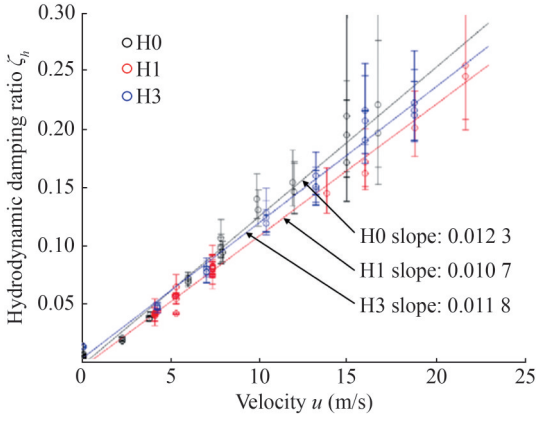

Figure 10 HDRs at different velocities for three different hydrofoils (H0, H1, and H3) (Seeley et al., 2012)

1981), and cylinder (Vandiver and Chung, 1989) showed that the HDRs almost remained unchanged. In the experimental work of Roth et al. (2009), the HDR increased linearly with velocity when the velocity ranged from 3 m/s to 15 m/s but remained constant when the velocity was within 3 m/s. Based on experimental phenomena, Yao et al. (2014) summarized that the HDR increased linearly with the flow velocity and remained unchanged when the flow velocity was above and below the resonant flow velocity, respectively. The experiment of Bergan et al. (2019) supported the aforementioned result.

3) The HDR displays a sharp drop in the lock-in region. This region indicates that the vortex shedding frequency was locked onto the structural eigenfrequency over a wide range of free-stream velocity (Ausoni, 2009; Liu et al., 2023). Therefore, the resonance resulted in a sufficiently large response amplitude. In particular, the reduction in HDR could reach an order of magnitude in the presence of lock-in, as shown in Figure 11 (Reese, 2010). The negative HDR can also be observed (Zeng et al., 2021b) in the lock-in region of the torsional mode of a hydrofoil.

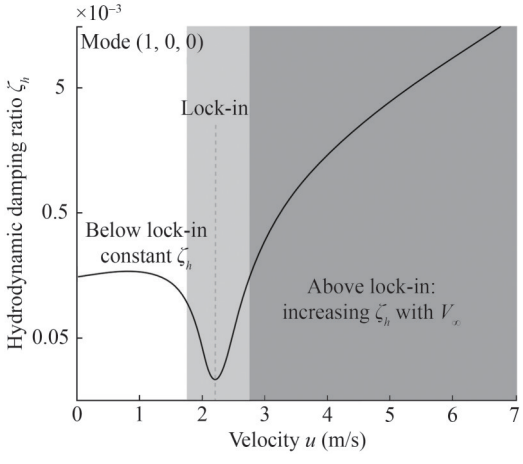

Figure 11 Hydrodynamic damping ratio with increasing velocity, adapted from Reese (2010)

4.2 Effect of AOA

The AOA inevitably exists under off-design conditions, and its effect on the modal parameter of blade-like structures also attracted increasing attention (Ducoin et al., 2009; 2012). Reese (2010) and Ducoin et al. (2012) measured the vibration response of a hydrofoil and found that the natural frequency almost remained the same when the AOA ranged from 2° to 8°, indicating the independence of the fluid added from the AOA. Considering the hydrodynamic behavior, the existence of the AOA changes the pressure distribution on the blade, thereby affecting the oscillation of the structure. For example, the experiment of Reese (2010) indicated that the HDR was varied at the AOA of 0°, 4°, −4°, and 10°. Zeng et al. (2021b) obtained the HDRs of a NACA 0009 hydrofoil at different velocities when the AOA ranged from 0° to 6°. Their results showed that the AOA slightly affected the HDR when the velocity was below the resonant velocity, and the HDR decreased with increasing AOA when the velocity was above the resonant velocity.

4.3 Effect of gap

The gap in the current investigation is defined as the distance between the blade and the rigid wall. The small gap has the advantage of energy leakage reduction, resulting in hydraulic machinery with superior performance (Xu et al., 2017). Regarding the vibration characteristic, if the distance between the underwater vibrating structure and the rigid wall was farther, then the fluid-added mass would decrease, thereby increasing the natural frequency (He et al., 2019; Rodriguez et al., 2012). Torre et al. (2014) found that the gap increased from 0.08% of the span width to 1.43% when the reduction of the natural frequency of hydrofoil reached 12.19%. Considering the HDR, this frequency also gradually decreased with the increasing gap (Harrison et al., 2007; Naik et al., 2003). Specifically, the decreasing trend conformed to the asymptote function; that is, the HDR hardly decreased when the gap was sufficiently large (Zeng et al., 2021a). In the case of a disk, the reduction of HDR reached 31.52% when the gap increased from 0.67% to 3.33% radius, and the reduction was only 4.72% when the gap increased from 16.67% to 26.67% radius (Zeng et al., 2023a). The behavior between the HDR and gap remained the same for different fluid media, such as water, acetone, and oil (Valentin et al., 2014). Therefore, from the perspective of suppressing vibration, a small gap is also recommended in actual engineering.

4.4 Effect of rotation

Centrifugal and Coriolis forces are theoretically introduced during structure rotation, resulting in highly complex vibration characteristics. The centrifugal force generated by rotation was applied to the structure in the form of a prestress,

thereby affecting the natural frequency of the structure in the water (Qiao et al., 2023). Two peaks were detected for the frequency domain of each diametrical mode at rotating conditions, while only one peak was observed at nonrotating conditions (Louyot et al., 2020). In particular, the frequency difference between the two peaks was linearly increased with the rising rotational speed (Presas et al., 2015).

For the HDR at different rotational speeds, the experimental results of a disk are shown in Figure 12 (Weder et al., 2019). The HDR was increased with rotating speed for the low-order modes, which corresponded with the behavior of a propeller (Chen et al., 2020a). Meanwhile, for some high-order modes in Figure 12, the HDR was found to be independent of the rotational speed. Similarly, Zeng et al. (2023a) revealed that the HDR of the eight-diametrical mode also remained almost unchanged when the rotational speed increased from 240 r/min to 600 r/min.

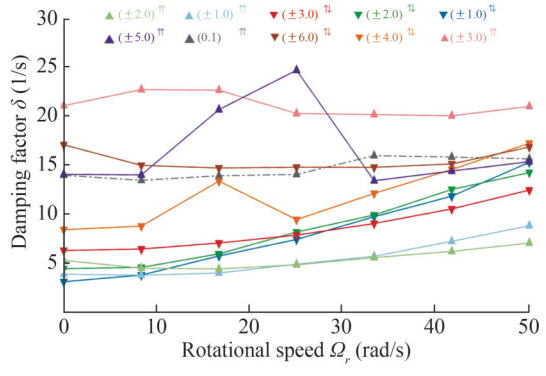

Figure 12 HDRs at different rotational speeds (Weder et al., 2019)

Increasing the rotational speed raises the relative flow velocity in terms of structure. The pressure and shear stress experienced by the underwater structure will also increase with the rotational speed, which can explain the increase in HDR with the rotational speed. Meanwhile, the characteristics of HDR at different rotational speeds must be further revealed for some high-order modes. In addition, the consistency of the adjacent modes under sufficiently large rotational stalls remains unclear, and determining their impact on HDR is also difficult.

4.5 Effect of leading-edge cavitation

Cavitation, which is crucial in the FSI, occurs when the local pressure is lower than the saturated vapor pressure (Wen et al., 2023b; Sun et al., 2022). On the one hand, the fluid in contact with the structure was switched from liquid to vapor, resulting in a reduction of the fluid-added mass (Liu et al., 2017; Roig et al., 2021; Wen et al., 2023a). In particular, the added mass could decrease to 72% of that without cavitation when the leading cavitation length was greater than the half chord length (Torre et al., 2013). On the other hand, changes in the boundary layer characteristics and the introduction of additional excitation frequencies can be attributed to cavitation, revealing the impact of cavitation on HDR and attracting widespread attention (Zeng et al., 2022c; Wang, 2020; Gaschler and Abdel-Maksoud, 2014). The impact of cavitation on HDR can be divided into the following three situations:

1) The HDR decreases with increasing cavity length if the velocity is above the resonant velocity. This behavior was observed in the experimental work of Zeng et al. (2022c), and this phenomenon was independent of AOA, as shown in Figure 13. The simulation work of Wang (2020) also proved a considerable reduction in HDR in the presence of cavitation.

2) The HDR in the lock-in region may increase as the cavity length decreases. This phenomenon was found through experimentation (Zeng et al., 2022c) and simulation (Roig et al., 2021) revealing that the resonance was staggered as the cavitation changed the natural frequencies.

3) The effect of cavitation on the HDR when the velocity is below the resonant velocity is negligible. In particular, the HDR for the first torsional mode of a hydrofoil remained constant when the cavitation length was from 0 to approximately 0.95 times the chord length (Zeng et al., 2022c). Similar results were also obtained in the case of a propeller (Gaschler et al., 2014).

Despite the established quantitative relationships between leading-edge cavitation and HDR, the internal flow mechanisms remain unclear. Simplifying leading-edge cavitation into cavitation bubbles and exploring the mutual mechanisms between bubble dynamics, structural vibration, and energy loss can help reduce the complexity of cavitation. Zhang et al. (2023) recently established a universal theory for the dynamics of oscillating bubbles by considering the viscosity, bubble interaction, and surface tension, which was carefully validated by comparing the experimental results. Especially on different scales and boundaries, the theory proposed by Zhang et al. (2023) demonstrated good applicability. This finding further indicates that the influence mechanism of cavitation on HDR can be explored from the perspective of cavitation bubble dynamics in future work.

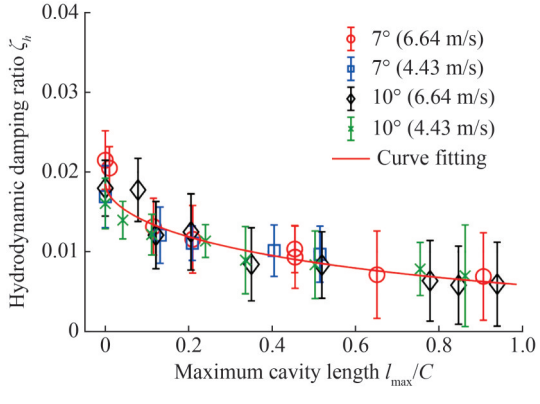

Figure 13 HDRs at different leading-edge cavitation lengths when the velocity is above the resonant velocity (Zeng et al., 2022c)

5 Prediction formulas of the HDR

The construction of the HDR prediction formula is conducive to improving the efficiency of vibration analysis in the design stage and saving numerical calculation resources (Tita et al., 2001; Chin and Lau, 2012). The main methods can be divided into theoretical derivation and semi-empirical formula construction.

5.1 Theoretical derivation

Blake et al. (1972) disregarded the effects of viscosity and structural modal mass and proposed an HDR theoretical prediction formula for hydrofoils based on two-dimensional assumptions. They revealed the relationship between HDR and flow velocity, chord length, and natural frequencies in air and water as follows:

$$\zeta_h = \gamma \frac{u}{2\pi f_{\mathrm{nw}} c} + \zeta_{\mathrm{stat}} \tag{21}$$

where u is the incoming flow velocity, f_{nw} is the natural frequency in water, c is the chord length, and $\gamma = 0.5$ and 2 for the bending and torsional modes, respectively. ζ_{stat} is the HDR in still water.

Compared with the experimental results, the prediction formula proposed by Blake et al. (1973) could successfully reflect the linear relationship between the HDR of a hydrofoil and flow velocity but overpredicted the HDR. Based on the work of Blake et al. (1973), Reese (2010) considered the impact of structural modal mass on HDR, which was theoretically more complete, as shown below:

$$\zeta_h = \gamma \frac{u}{2\pi f_{\mathrm{nw}} c}\left[1 - \left(\frac{f_{\mathrm{nw}}}{f_{\mathrm{na}}}\right)^2\right] + \zeta_{\mathrm{stat}} \tag{22}$$

where f_{na} is the natural frequency in air.

Kamier and Kavitskii (1976) applied the theoretical prediction formula of aerodynamic damping to HDR prediction (Equation (23)). The linear growth trend of HDR with flow velocity was also consistent with the experiment data.

$$\zeta_h = \frac{\pi}{2} \frac{u \rho_f c}{m f_{\mathrm{nw}}} G\left(S_{t,h}\right) + \zeta_{\mathrm{stat}} \tag{23}$$

where ρ_f is the fluid density and $G\left(S_{t,h}\right)$ is a constant related to the Strouhal number.

Bahrami et al. (2023) focused on flow parameters in the near-wall region for the flat plate and introduced a universal HDR prediction formula that was independent of structural mode shapes as follows:

$$\zeta_h = \left(\frac{4}{\pi}\right)\frac{\delta_s}{L} \tag{24}$$

where L is the characteristic length and δ_s is the Stokes length relative to the Reynolds number.

5.2 Semi-empirical formula construction

Combining experimental results and theoretical derivation, the construction of semi-empirical prediction formulas for HDR has also received widespread attention. For example, considering viscosity for disks based on kinetic energy theory and coupling experimental results, Santo et al. (1981) constructed a prediction formula for HDR. Vandiver and Chung et al. (1989) conducted a theoretical derivation of HDR for submarine cables. They considered the effects of fluid-added mass and resistance when expressing the formula and calibrated some key parameters based on experimental results. Considering the theoretical works of Reese (2010), Bergan (2019) combined a large number of experimental results to establish a semi-empirical prediction formula for the HDR, as shown below:

$$\zeta_h = 0.873 \frac{u}{f_{\mathrm{nw}}} + \zeta_{\mathrm{stat}} \tag{25}$$

Comparing existing HDR prediction formulas, despite inconsistency in form, the relationships with key parameters are generally consistent. HDR was generally believed to be directly proportional to the incoming flow velocity and inversely proportional to the natural frequency of water. In addition, the previously published references showed that flow situations, such as lock-in (Zeng et al., 2021b), AOA (Zeng et al., 2021b), gap (Xiu et al., 2018), and cavitation (Roig et al., 2021), also had a remarkable influence on HDR. Therefore, Zeng et al. (2023b) introduced a comprehensive semi-empirical formula by combining theoretical derivation and HDR results with different flow parameters:

$$\zeta_h = \begin{cases} \zeta_{\mathrm{stat}} & u^* \leqslant u_1^* \\ -(\zeta_{\mathrm{stat}})\mathrm{e}^{\left[-18\left(\frac{u^* - u_r^*}{\Delta u^*}\right)^2\right]} + \zeta_{\mathrm{stat}} & u_1^* < u^* \leqslant u_2^* \\ \gamma \dfrac{u^*}{2\pi}\left[1 - \left(\dfrac{f_{\mathrm{nw}}}{f_{\mathrm{na}}}\right)^2\right] f(\alpha) f\left(d_r\right) f(\sigma) + \zeta_{\mathrm{stat}} & u^* > u_2^* \end{cases} \tag{26}$$

$$u^* = \frac{u}{f_{\mathrm{nw}} c} \tag{27}$$

where u^* is the reduced velocity; u_1^* and u_2^* are the initiation and termination velocities of the lock-in region, respectively. u_r^* is the resonant velocity; in the absence of lock-in, then u_1^*=u_2^*=u_r^*. The $f(\alpha)$, $f\left(d_r\right)$, and $f(\sigma)$ are the AOA, gap, and cavitation correction terms, respectively.

6 Conclusions and future works

6.1 Conclusions

The current study aims to review the HDR characteristics of a blade-like structure, emphasizing the quantitatively determined methods and influencing factors.

1) The detailed processes were introduced for the experiments, and multiple HDR identification methods were compared. The logarithmic decay and half-power bandwidth methods were recommended for the free and forced vibrations, respectively. The Hilbert transform method was recommended for the time-varying HDR.

2) The solving equations of three different methods were provided for the simulations, and the corresponding calculation accuracy and efficiency were discussed. The modal work method considers calculation accuracy and efficiency and has good applicability to rotating machinery.

3) The key flow parameters affecting the HDR, including incoming flow velocity, the AOA, the gap, the rotation speed, and leading-edge cavitation, were summarized. The HDR prediction formulas under different flow parameters were then introduced.

6.2 Future works

1) Increasing the HDR of the blade-like structure will suppress the resonance amplitude, thereby improving the operating stability of the unit. However, attention to the structural optimization design aimed at increasing HDR is still lacking.

2) When the flow velocity is below or above the resonant velocity, several previous experiments have demonstrated inconsistencies in the behavior of HDR with flow velocity. Therefore, understanding the energy dissipation mechanism during the resonant situation is necessary.

3) Most experiments were conducted on blade-like structures. From a practical engineering perspective, evaluating the HDR of the complete prototype runner is valuable.

4) Current research has shown that rotation will cause two natural frequencies in each diametrical mode, and their frequency difference will increase with the rotational speed. A sufficiently large rotational speed may cause the coincidence of two adjacent diametrical modes. Thus, determining the HDR characteristics is crucial.

Funding Supported by the National Natural Science Foundation of China (Nos. 52222904 and 52309117), and China Postdoctoral Science Foundation (Nos. 2022TQ0168 and 2023M731895).

Competing interest The authors have no competing interests to declare that are relevant to the content of this article.

References

Anthony D, Simón F (2012) Accuracy and robustness of four basic single degree of freedom methods for determining the modal parameters of non-lightly damped systems. Journal of Sound and Vibration 331(24): 5191-5208. DOI: 10.1016/j.jsv.2012.06.015

Aquelet N, Souli M (2003) Damping effect in fluid-structure interaction: Application to slamming problem. ASME Pressure Vessels and Piping Conference, Cleveland

Ausoni P (2009) Turbulent vortex shedding from a blunt trailing edge hydrofoil. PhD thesis, Swiss Federal Institute of Technology Lausanne, Lausanne

Bahrami M, Cervantes M, Raisee M, Nourbakhsh A (2023) Hydrodynamic damping in laminar, transient and turbulent regimes: Analytical and computational study. Ocean Engineering 289: 116277. DOI: 10.1016/j.oceaneng.2023.116277

Bai X, Li B, Xu X, Xiao Y (2022) A review of current research and advances in unmanned surface vehicles. Journal of Marine Science and Application 21(2): 47-58. DOI: 10.1007/s11804-022-00276-9

Bergan C, Solemslie B, Østby P, Dahlhaug O (2018a) Hydrodynamic damping of a fluttering hydrofoil in high-speed flows. International Journal of Fluid Machinery and Systems 11(2): 146-153. DOI: 10.5293/IJFMS.2018.11.2.146

Bergan C, Tengs E, Solemslie B, Dahlhaug O (2018b) An experimental investigation of the hydrodynamic damping of vibrating hydrofoils. IOP Conference Series: Earth and Environmental Science 240(6): 062008. DOI: 10.1088/1755-1315/240/6/062008

Bergan C, Tengs E, Solemslie B, Dahlhaug O (2019) Damping measurements on a multi-blade cascade with multiple degrees of freedom: a francis-99 test case. Journal of Physics Conference Series 1296: 012003. DOI: 10.1088/1742-6596/1296/1/012003

Blake W (1972) On the damping of transverse motion of free-free beams in dense stagnant fluids. Shock and Vibration Bulletin 42(4): 41-55

Blake W, Maga L (1973) Vibration dynamics of flow-excited structs in water. Naval Ship Research and Development Center, Bethesda, Report

Bulatovic R (2002) On the critical damping in multi-degree-of-freedom systems. Mechanics Research Communications 29(5): 315-319. DOI: 10.1016/S0093-6413(02)00263-X

Cha Y, Chae W, Kim H, Walcott H, Peterson S, Porfiri M (2016) Energy harvesting from a piezoelectric biomimetic fish tail. Renewable Energy 86: 449-458. DOI: 10.1016/j.renene.2015.07.077

Chaplin J, Subbiah K (1998) Hydrodynamic damping of a cylinder in still water and in a transverse current. Applied Ocean Research 20(4): 251-259. DOI: 10.1016/S0141-1187(98)00023-6

Chaplin JR (2000) Hydrodynamic damping of a cylinder at $\beta \approx 10^6$.

Journal of Fluids and Structures 14(8): 1101-1117. DOI: 10.1006/jfls.2000.0318

Chen H, Aït-Ahmed N, Zaïm E, Machmoum M (2012) Marine tidal current systems: state of the art. 2012 IEEE International Symposium on Industrial Electronics, 1431-1437. DOI: 10.1109/ISIE.2012.6237301

Chen H, Tang T, Aït-Ahmed N, Benbouzid M, Machmoum M, Zaïm M (2018) Attraction, challenge and current status of marine current energy. IEEE Access 6: 12665-12685. DOI: 10.1109/ACCESS.2018.2795708

Chen H, Tong X, He Z, Chen Y (2020a) Numerical and experimental studies on the hydrodynamic damping of a zero-thrust propeller. Journal of Fluids and Structures 94: 102957. DOI: 10.1016/j.jfluidstructs.2020.102957

Chen P, Chen J, Hu Z (2020b) Review of experimental-numerical methodologies and challenges for floating offshore wind turbines. Journal of Marine Science and Application 19: 339-361. DOI: 10.1007/s11804-020-00165-z

Chen S, Jendrzejczyk J (1981) Flow velocity dependence of damping in tube arrays subjected to liquid cross-flow. Journal of Fluids Engineering 103(5): 130-135. DOI: 10.1115/1.3263377

Chin C, Lau M (2012) Modeling and testing of hydrodynamic damping model for a complex-shaped remotely-operated vehicle for control. Journal of Marine Science and Application 11: 150-163. DOI: 10.1007/s11804-012-1117-2

Coutu A, Seeley C, Monette C, Nennemann B, Marmont H (2012) Damping measurements in flowing water. IOP Conference Series: Earth and Environmental Science 15(4): 062060. DOI: 10.1088/1755-1315/15/6/062060

Crandall S (1970) The role of damping in vibration theory. Journal of Sound and Vibration 11(1): 3-18. DOI: 10.1016/S0022-460X(70)80105-5

Čupr P, Štefan D, Habán V, Rudolf P (2019) FSI analysis of francis-99 hydrofoil employing SBES model to adequately predict vortex shedding. Journal of Physics: Conference Series 1296: 012002. DOI: 10.1088/1742-6596/1296/1/012002

Dehkharqani A, Aidanpää J, Engström F, Cervantes M (2018) A review of available methods for the assessment of fluid added mass, damping, and stiffness with an emphasis on hydraulic turbines. Applied Mechanics Reviews 70(5): 050801. DOI: 10.1115/1.4042279

Ducoin A, Astolfi J, Deniset F, Sigrist J (2009) Computational and experimental investigation of flow over a transient pitching hydrofoil. European Journal of Mechanics-B/Fluids 28(6): 728-743. DOI: 10.1016/j.euromechflu.2009.06.001

Ducoin A, Astolfi J, Gobert M (2012) An experimental study of boundary-layer transition induced vibrations on a hydrofoil. Journal of Fluids and Structures 32: 37-51. DOI: 10.1016/j.jfluidstructs.2011.04.002

Fraenkel P (2002) Power from marine currents. Proceedings of the Institution of Mechanical Engineers, Part A: Journal of Power and Energy 216(1): 1-14. DOI: 10.1243/0957650027600247

Gaschler M, Abdel-Maksoud M (2014) Computation of hydrodynamic mass and damping coefficients for a cavitating marine propeller flow using a panel method. Journal of Fluids and Structures 49: 574-593. DOI: 10.1016/j.jfluidstructs.2014.06.001

Gauthier J, Giroux A, Etienne S, Gosselin F (2017) A numerical method for the determination of flow-induced damping in hydroelectric turbines. Journal of Fluids and Structures 69: 341-354. DOI: 10.1016/j.jfluidstructs.2017.01.004

Harrison C, Tavernier E, Vancauwenberghe O (2007) On the response of a resonating plate in a liquid near a solid wall. Sensors and Actuators A: Physical 134(2): 414-426. DOI: 10.1016/j.sna.2006.06.023

He L, Wang Z, Kurosawa S, Nakahara Y (2014) Resonance investigation of pump-turbine during startup process. IOP Conference Series: Earth and Environmental Science 22(3): 032024. DOI: 10.1088/1755-1315/22/3/032024

He L, Zhou L, Ahn S, Wang Z, Nakahara Y, Kurosawa S (2019) Evaluation of gap influence on the dynamic response behavior of pump-turbine runner. Engineering Computations 36(2): 491-508. DOI: 10.1108/EC-04-2018-0169

Jacobson K, Kiviaho J, Kennedy G, Smith M (2019) Evaluation of time-domain damping identification methods for flutter-constrained optimization. Journal of Fluids and Structures 87: 174-188. DOI: 10.1016/j.jfluidstructs.2019.03.011

Kaminer A, Kavitskii B (1976) Experimental investigation of hydrodynamic damping during bending oscillations of blade profiles in water flow. Strength of Materials 8(1): 25-2. DOI: 10.1007/BF01528208

Kohtanen E, Davis R (2019) Hydroelastic damping of low aspect ratio cantilevered plates. Journal of Fluids and Structures 90: 315-333. DOI: 10.1016/j.jfluidstructs.2019.06.015

Liaghat T, Guibault F, Allenbach L, Nennemann B (2014) Two-way fluid-structure coupling in vibration and damping analysis of an oscillating hydrofoil. Proceedings of the ASME 2014 International Mechanical Engineering Congress and Exposition, Quebec

Liang Q, Rodrıguez C, Egusquiza E, Escaler X, Farhat M, Avellan F (2007) Numerical simulation of fluid added mass effect on a francis turbine runner. Computing Fluids 36(6): 1106-1118. DOI: 10.1016/j.compfluid.2006.08.007

Liu X, Luo Y, Karney B, Wang Z, Zhai L (2015) Virtual testing for modal and damping ratio identification of submerged structures using the PolyMAX algorithm with two-way fluid – structure Interactions. Journal of Fluids and Structures 54: 548-565. DOI: 10.1016/j.jfluidstructs.2015.01.001

Liu X, Zhou L, Escaler X, Wang Z, Luo Y, Torre O (2017) Numerical simulation of added mass effects on a hydrofoil in cavitating flow using acoustic fluid–structure interaction. Journal of Fluids Engineering 139(4): 041301. DOI: 10.1115/1.4035113

Liu Y, Berger T, Huang B, Wu Q, Farhat M (2023) Vortex shedding from a composite hydrofoil: Experimental evidence of a novel "partial lock-in". Physics of Fluids 35(12): 125132. DOI: 10.1063/5.0184582

Louyot M, Nennemann B, Monette C, Gosselin F (2020) Modal analysis of a spinning disk in a dense fluid as a model for high head hydraulic turbines. Journal of Fluids and Structures 94: 102965. DOI: 10.1016/j.jfluidstructs.2020.102965

Maung P, Prusty B, Shamsuddoha M, Phillips A, St John N (2021) Static and dynamic response of a carbon composite full-scale hydrofoil manufactured using automated fibre placement. Composites Part C: Open Access 6: 100218. DOI: 10.1016/j.jcomc.2021.100218

Monette C, Nennemann B, Seeley C, Coutu A, Marmont H (2014) Hydrodynamic damping theory in flowing water. IOP Conference Series: Earth and Environmental Science 22(3): 032044. DOI: 10.1088/1755-1315/22/3/032044

Nachtane M, Tarfaoui M, Goda I, Rouway M (2020) A review on the technologies, design considerations and numerical models of tidal current turbines. Renewable Energy 157: 1274-1288. DOI: 10.1016/j.renene.2020.04.155

Naik T, Longmire E, Mantell S (2003) Dynamic response of a cantilever in liquid near a solid wall. Sensors and Actuators A: Physical 102(3): 240-254. DOI: 10.1016/S0924-4247(02)00398-9

Nennemann B, Monette C, Chamberland-lauzon J (2016) Hydrodynamic damping and stiffness prediction in Francis turbine runners using CFD. IOP Conference Series: Earth and Environmental Science 49(7): 072006. DOI: 10.1088/1755-1315/49/7/072006

Nicholls-Lee R, Turnock S, Boyd S (2011) A method for analysing fluid structure interactions on a horizontal axis tidal turbine. 9th European Wave and Tidal Energy Conference, Southampton

Pernod L, Ducoin A, Le Sourne H, Astolfi J, Casari P (2019) Experimental and numerical investigation of the fluid-structure interaction on a flexible composite hydrofoil under viscous flows. Ocean Engineering 194: 106647. DOI: 10.1016/j.oceaneng.2019.106647

Presas A, Egusquiza E, Valero C, Valentin D, Seidel U (2014) Feasibility of using PZT actuators to study the dynamic behavior of a rotating disk due to rotor-stator interaction. Sensors 14(7): 11919-11942. DOI: 10.3390/s140711919

Presas A, Valentin D, Egusquiza E, Valero C, Egusquiza M, Bossio M (2017) Accurate determination of the frequency response function of submerged and confined structures by using PZT-patches. Sensors 17(3): 660. DOI: 10.3390/s17030660

Presas A, Valentin D, Egusquiza E, Valero C, Seidel U (2015) Influence of the rotation on the natural frequencies of a submerged-confined disk in water. Journal of Sound and Vibration 337: 161-180. DOI: 10.1016/j.jsv.2014.10.032

Presas A, Valentin D, Egusquiza E, Valero C, Seidel U (2016) Dynamic response of a rotating disk submerged and confined. Influence of the axial gap. Journal of Fluids and Structures 62: 332-349.

Presas A, Valentin D, Valero C, Egusquiza M, Egusquiza E (2019) Experimental measurements of the natural frequencies and mode shapes of rotating disk-blades-disk assemblies from the stationary frame. Applied Sciences 9(18): 3864. DOI: 10.3390/app9183864

Qiao F, Sun Y, Zhu D, Fang M, Zhang F, Tao R, Xiao R (2023) Analysis of stress–strain characteristics and signal coherence of low-specific-speed impeller based on fluid – structure interaction. Journal of Marine Science and Engineering 12(1): 2. DOI: 10.3390/jmse12010002

Rankl C, Pastushenko V, Kienberger F, Stroh C, Hinterdorfer P (2004) Hydrodynamic damping of a magnetically oscillated cantilever close to a surface. Ultramicroscopy 100(4): 301-308. DOI: 10.1016/j.ultramic.2003.12.014

Reese M (2010) Vibration and damping of hydrofoils in uniform flow. Master thesis, The Pennsylvania State University, Pennsylvania

Rodriguez C, Flores P, Pierart F, Contzen L, Egusquiza E (2012) Capability of structural–acoustical FSI numerical model to predict natural frequencies of submerged structures with nearby rigid surfaces. Computers & Fluids 64: 117-126. DOI: 10.1016/j.compfluid.2012.05.011

Roig R, Chen J, Torre O, Escaler X (2021) Understanding the influence of wake cavitation on the dynamic response of hydraulic profiles under lock-in conditions. Energies 14(19): 6033. DOI: 10.3390/en14196033

Roth S (2012) Fluid-structure coupling effects on the dynamic response of pump-turbine guide vanes. PhD thesis, Swiss Federal Institute of Technology Lausanne, Lausanne

Roth S, Calmon M, Farhat M, Münch C, Bjoern H, Avellan F (2009) Hydrodynamic damping identification from an impulse response of a vibration blade. 3rd IAHR International Meeting of the Workgroup on Cavitation and Dynamic Problems in Hydraulic Machinery and Systems, Brno

Santo F (1981) Added mass and hydrodynamic damping of perforated plates vibrating in water. Journal of Pressure Vessel Technology 103(2): 175-182. DOI: 10.1115/1.3263384

Seeley C, Coutu A, Monette C, Nennemann B, Marmont H (2012) Characterization of hydrofoil damping due to fluid–structure interaction using piezocomposite actuators. Smart Materials and Structures 21(3): 035027. DOI: 10.1088/0964-1726/21/3/035027

Silva D (2000) Vibration: fundamentals and practice. CRC Press, Boca Raton

Sun Y, Yao Z, Wen H, Zhong Q, Wang F (2022) Cavitation bubble collapse in a vicinity of a rigid wall with a gas entrapping hole. Physics of Fluids 34(7): 073314. DOI: 10.1063/5.0096986

Tengs E (2019) Numerical simulation of fluid-structure Interaction in high head Francis turbines. PhD thesis, Norwegian University of Science and Technology, Trondheim

Tengs E, Bergan C, Jakobsen K, Storli P (2019) Numerical simulation of the hydrodynamic damping of a vibrating hydrofoil. IOP Conference Series: Earth and Environmental Science 240(6): 062002. DOI: 10.1088/1755-1315/240/6/062002

Tita V, Carvalho J, Lirani J (2001) A procedure to estimate the dynamic damped behavior of fiber reinforced composite beams submitted to flexural vibrations. Materials Research 4: 315-321. DOI: 10.1590/S1516-14392001000400015

Torre O, Escaler X, Egusquiza E, Farhat M (2013) Experimental investigation of added mass effects on a hydrofoil under cavitation conditions. Journal of Fluids and Structures 39: 173-187. DOI: 10.1016/j.jfluidstructs.2013.01.008

Torre O, Escaler X, Egusquiza E, Farhat M (2014) Numerical and experimental study of a nearby solid boundary and partial submergence effects on hydrofoil added mass. Computers & Fluids 91: 1-9. DOI: 10.1016/j.compfluid.2013.12.003

Trivedi C (2017) A review on fluid structure interaction in hydraulic turbines: A focus on hydrodynamic damping. Engineering Failure Analysis 77: 1-22. DOI: 10.1016/j.engfailanal.2017.02.021

Valentin D, Presas A, Egusquiza E, Valero C (2014) Experimental study on the added mass and damping of a disk submerged in a partially fluid-filled tank with small radial confinement. Journal of Fluids and Structures 50: 1-17. DOI: 10.1016/j.jfluidstructs.2014.06.006

Vandiver J, Chung T (1989) Hydrodynamic damping on flexible cylinders in sheared flow. Journal of Waterway, Port, Coastal, and Ocean Engineering 115(2): 154-171. DOI: 10.4043/5524-MS

Wang J, Wan D (2020) Application progress of computational fluid dynamic techniques for complex viscous flows in ship and ocean engineering. Journal of Marine Science and Application 19: 1-16. DOI: 10.1007/s11804-020-00124-8

Wang W (2020) Effect of cavitation on the dynamic characteristics of hydraulic machinery structures. PhD thesis, China Agricultural University, Beijing

Wang W, Zhou L, Xia X, Tao R (2021a) Analysis of the hydrodynamic damping characteristics on a symmetrical hydrofoil. Renewable Energy 178: 821-829. DOI: 10.1016/j.renene.2021.06.026

Wang Y, Niu W, Yu X, Yang S, Zhang L (2021b) Quantitative evaluation of motion performances of underwater gliders considering ocean currents. Ocean Engineering 236: 109501. DOI: 10.1016/j.oceaneng.2021.109501

Weder M, Horisberger B, Monette C, Sick M, Dual J (2019) Experimental modal analysis of disk-like rotor–stator system coupled by viscous liquid. Journal of Fluids and Structures 88: 198-215. DOI: 10.1016/j.jfluidstructs.2019.05.003

Wen H, Yao Z, Wu Q, Sun Y, Yang C, Zhong Q (2023a) Investigation

of cavitation erosion caused by laser-induced single bubble collapse near alloy coating surface. Journal of Hydrodynamics 35: 876-886. DOI: 10.1007/s42241-023-0062-7

Wen H, Yao Z, Zhong Q, Tian Y, Sun Y, Wang F (2023b) Energy partitioning in laser-induced millimeter-sized spherical cavitation up to the fourth oscillation. Ultrasonics Sonochemistry 95: 106391. DOI: 10.1016/j.ultsonch.2023.106391

Wu J, Liu Y, Zhang D, Cao Z, Guo Z (2022) Numerical investigation of vortex shedding from a 5: 1 rectangular cylinder at different angles of attack. Journal of Marine Science and Engineering 10(12), 1913. DOI: 10.3390/jmse10121913

Xie T, Wang T, He Q, Diallo D, Claramunt C (2020) A review of current issues of marine current turbine blade fault detection. Ocean Engineering 218: 108194. DOI: 10.1016/j.oceaneng.2022.111299

Xiu H, Davis R, Romeo R (2018) Edge clearance effects on the added mass and damping of beams submerged in viscous fluids. Journal of Fluids and Structures 83: 194-217. DOI: 10.1016/j.jfluidstructs.2018.08.016

Xu Y, Tan L, Liu Y, Cao S (2017) Pressure fluctuation and flow pattern of a mixed-flow pump with different blade tip clearances under cavitation condition. Advances in Mechanical Engineering 9(4): 1-12. DOI: 10.1177/1687814017696227

Yang J, Marks C, Jiang J, Chen D, Elahi A, Tsai W (1985) Determination of fluid damping using random excitation. Journal of Energy Resources Technology 107(2): 220. DOI: 10.1115/1.3231180

Yao Z, Wang F, Dreyer M, Farhat M (2014) Effect of trailing edge shape on hydrodynamic damping for a hydrofoil. Journal of Fluids and Structures 51: 189-198. DOI: 10.1016/j.jfluidstructs.2014.09.003

Younes M, Younes Y, El-Madah M, Ibrahim I, El-Dannanh E (2007) An experimental investigation of hydrodynamic damping due to vertical baffle arrangements in a rectangular tank. Proceedings of the Institution of Mechanical Engineers, Part M: Journal of Engineering for the Maritime Environment 221(3): 115-123. DOI: 10.1243/14750902JEME59

Zeng Y, Qi X, Bai M, Zhou L, Yao Z (2023a) How the radial gap affects the runner's hydrodynamic damping characteristic of a pump-turbine: A physical experiment on a rotating disc. Journal of Hydrodynamics 35(4): 736-745. DOI: 10.1007/s42241-023-0058-3

Zeng Y, Qi X, Shu L, Yao Z, Zhou L, Wang F (2022a) Fluid–structure interaction effects of a partially immersed, cantilevered hydrofoil. Journal of Fluids Engineering 144(2): 021202. DOI: 10.1115/1.4051859

Zeng Y, Qi X, Yao Z, Wang F, Wang Y, Wang F (2022b) Experimental investigation on damping characteristics of a vibrating hydrofoil in low-order modes. Journal of Mechanical Engineering 58(5): 108-118. (in Chinese) DOI: 10.3901/JME.2022.05.108

Zeng Y, Wang C, Huang B, Wang F, Xiao R, Yao Z (2023b) A comprehensive empirical equation for the hydrodynamic damping of vibrating blade-like structures. Ocean Engineering 270: 113721. DOI: 10.1016/j.oceaneng.2023.113721

Zeng Y, Yao Z, Gao J, Hong Y, Wang F, Zhang F (2019a) Numerical investigation of added mass and hydrodynamic damping on a blunt trailing edge hydrofoil. Journal of Fluids Engineering 141(8): 081108. DOI: 10.1115/1.4042759

Zeng Y, Yao Z, Huang B, Wu Q, Wang F (2022c) Experimental investigation of the hydrodynamic damping of a vibrating hydrofoil in cavitating flow. Ocean Engineering 266: 112734. DOI: 10.1016/j.oceaneng.2022.112734

Zeng Y, Yao Z, Hong Y, Wang F (2020) Research on numerical prediction methods of hydrodynamic damping ratio for a hydrofoil based on one-way and two-way fluid-structure interactions. Journal of Hydraulic Engineering 51(11): 1432-1439. (in Chinese) DOI: 0559-9350(2020)11-1432-08

Zeng Y, Yao Z, Zhang S, Wang F, Xiao R (2021a) Influence of Tip clearance on the hydrodynamic damping characteristics of a hydrofoil. Journal of Fluids Engineering 143(6): 061202. DOI: 10.1115/1.4049675

Zeng Y, Yao Z, Zhou P, Wang F, Hong Y (2019b) Numerical investigation into the effect of the trailing edge shape on added mass and hydrodynamic damping for a hydrofoil. Journal of Fluids and Structures 88: 167-184. DOI: 10.1016/j.jfluidstructs.2019.05.006

Zeng Y, Zhang M, Du Y, Yao Z, Wu Q, Wang F (2021b) Influence of attack angle on the hydrodynamic damping characteristic of a hydrofoil. Ocean Engineering 238: 109692. DOI: 10.1016/j.oceaneng.2021.109692

Zhang A, Li S, Cui P, Li S, Liu Y (2023) A unified theory for bubble dynamics. Physics of Fluids 35(3): 033323. DOI: 10.1063/5.0145415

Zhang M, Mbango-Ngoma P., Xiao Z, Qing G (2021) Numerical investigation of the trailing edge shape on the added damping of a Kaplan turbine runner. Mathematical Problems in Engineering 2021: 1-11. DOI: 10.1155/2021/9559454

Zhou J, Si Y, Chen Y (2023) A review of subsea AUV technology. Journal of Marine Science and Engineering 11(6): 1119. DOI: 10.3390/jmse11061119

Zhu D, Tao R, Lu Z, Wu Y, Xiao R (2022) Optimization design of the internal structural support of marine turbine blade for weight reduction: A preliminary study. Ocean Engineering 260: 111989. DOI: 10.1016/j.oceaneng.2022.111989

Zobeiri A (2012) Effect of hydrofoil trailing edge geometry on the wake dynamic. PhD thesis, Swiss Federal Institute of Technology Lausanne, Lausanne, Switzerland

Zobeiri A, Ausoni P, Avellan F, Farhat M (2012) How oblique trailing edge of a hydrofoil reduces the vortex-induced vibration. Journal of Fluids and Structures 32: 78-89. DOI: 10.1016/j.jfluidstructs.2011.12.003

Zrayka A, Mucchi E (2019) A comparison among modal parameter extraction methods. Applied Sciences 1: 1-11. DOI: 10.1007/s42452-019-0806-8